Talanta 91 (2012) 95–102

Contents lists available at SciVerse ScienceDirect

Talanta

journal homepage: www.elsevier.com/locate/talanta

Electrochemical immunosensor for carcinoembryonic antigen based on nanosilver-coated magnetic beads and gold-graphene nanolabels

Huafeng Chen[a,b], Dianping Tang[a,b,*], Bing Zhang[a,b], Bingqian Liu[a,b], Yuling Cui[a,b], Guonan Chen[a,b,*]

[a] Ministry of Education Key Laboratory of Analysis and Detection for Food Safety, Department of Chemistry, Fuzhou University, Fuzhou 350108, PR China
[b] Fujian Provincial Key Laboratory of Analysis and Detection Technology for Food Safety, Department of Chemistry, Fuzhou University, Fuzhou 350108, PR China

ARTICLE INFO

Article history:
Received 15 September 2011
Received in revised form 9 January 2012
Accepted 12 January 2012
Available online 18 January 2012

Keywords:
Bionanolabels
Carcinoembryonic antigen
Electrochemical immunosensor
Nanogold-decorated graphene nanosheets
Redox-active magnetic nanostructures

ABSTRACT

A novel redox-active magnetic nanostructure was synthesized by using a wet chemical method for high-efficiency electrochemical immunoassay of carcinoembryonic antigen (CEA, as a model analyte). The nanostructures based on the combination of a magnetic nanocore, a layer of electroactive poly(*o*-phenylenediamine) (PPD), and a silver metallic shell displayed good adsorption properties for the attachment of anti-CEA antibody selective to CEA. The magnetic nanostructure presented good redox behaviors to facilitate and modulate the way it was integrated into a magnetic carbon paste electrode. The assay was based on a sandwich-type immunoassay protocol by using nanogold-patterned graphene oxide nanoscales (AuNP-GO), conjugated with horseradish peroxidase-labeled anti-CEA, as secondary antibodies and biofunctionalized magnetic nanostructures as immunosensing probes. Under optimal conditions, the nanoparticle-based immunocomposites exhibited good electrochemical responses for the determination of CEA, and allowed the detection of CEA at a concentration as low as 1.0 pg mL^{-1} at a signal-to-noise ratio of 3. In addition, the magnetic immunosensing had good reproducibility, and acceptable accuracy, and could be successfully applied for the detection of CEA in the clinical serum specimens. Significantly, by controlling the target biomolecules, this assay can be easily extended for use with other immunosensings, and thus represents a versatile design routine.

1. Introduction

Nanocomposites, as a multiphase solid material, have broadened significantly to encompass a large variety of systems such as one-dimensional, two-dimensional, three-dimensional and amorphous materials, made of distinctly dissimilar components and mixed at the nanometer scale [1]. In mechanical terms, nanocomposites differ from conventional composite materials due to the exceptionally high surface-to-volume ratio of the reinforcing phase and/or its exceptionally high aspect ratio [2]. The general class of organic–inorganic nanocomposite materials is a fast growing area of research. Significant effort is focused on the ability to obtain the control of the nanoscale structures *via* innovative synthetic approaches [3]. The properties of nanocomposites depend not only on the properties of their individual parents but also on their morphology and interfacial characteristics [4].

Magnetic nanocomposites comprised of nano-sized magnetic crystals embedded in an amorphous matrix have been shown to have excellent soft magnetic properties [5,6]. Recently, researchers are attempting to join magnetic nanoparticles and fluorescent nanoparticles in a nanocomposite particle [7,8]. The fluorescent property can help the surgeon to better see the tumor while operating, while the magnetic property makes the tumor more visible during an MRI procedure done prior to surgery. *Vice versa*, magnetic nanocomposites were usually employed for the sensing fabrication in the electrochemical bioassays [9]. An important merit of magnetic nanomaterials is that they could be magnetically manipulated using permanent magnets or electromagnets, independent of normal microfluidic or biological processes [10,11]. Although magnetic beads-based sensing probes have been used for electrochemical immunoassays, most display low sensitivity and high background currents. Therefore, synthesis of new magnetic nanocomposites with redox activity and good biocompatibility is of great interest.

Silver nanoparticles, one of the strongest conductive nanomaterials, have attracted great attention due to their quantum characteristics of small granule diameter and large specific surface area as well as their ability to quickly transfer photoinduced electrons at the surfaces of colloidal particles [12,13]. Rijiravanich et al. reported a new method for electrochemical detection of DNA hybridization by using hollow polyelectrolyte shells

* Corresponding authors at: Ministry of Education Key Laboratory of Analysis and Detection for Food Safety, Department of Chemistry, Fuzhou University, Fuzhou 350108, PR China. Tel.: +86 591 22866125; fax: +86 591 22866135.
E-mail addresses: dianping.tang@fzu.edu.cn, dianping.tang@hotmail.com (D. Tang), gnchen@fzu.edu.cn (G. Chen).

0039-9140/$ – see front matter © 2012 Elsevier B.V. All rights reserved.
doi:10.1016/j.talanta.2012.01.025

bearing silver nanoparticles [14]. The immobilized silver nanoparticles on the hollow polyelectrolyte increased the conjugated amount of biomolecules, and strengthened the electron transfer. *o*-Phenylenediamine, an important precursor of many heterocyclic compounds, condenses with ketones and aldehydes to give rise to a variety of useful products [15]. Poly(*o*-phenylenediamine) (PPD), a polyaniline derivative, can be achieved through substituting hydrogen by an amino group in an aniline nucleus. The formed organic conducting PPD polymers naturally have both a pore size and a charged group that prevent interfering compounds from permeating them, so they have drawn wide interest in biosensor fabrication [16,17]. Compared to the other polymers such as polyacetylene, polypyrrole, polythiophene and polyaniline, poly(*o*-phenylenediamine) expresses good stability, high conductivity, many free amino and imino groups, unique trapezoidal, and semi-ladder structure [18]. Therefore, PPD has been employed for the preparation of the biosensors [19,20]. Moreover, the aromatic diamine polymers had a strong ability to adsorb the Ag(I) [21,22]. Based on the merits of silver nanoparticles and poly (*o*-phenylenediamine), we expect to synthesize a novel redox-active magnetic nanocomposite for improvement of electrochemical properties by using poly(*o*-phenylenediamine) as cross-linkage layer between magnetic nanoparticles and silver nanoparticles.

Carcinoembryonic antigen (CEA), a glycoprotein most often associated with colorectal cancer, used to monitor patients with this type of cancer. Most popular use is in early detection of relapse in individuals already treated for colorectal cancer [23]. The value of CEA in human serum is helpful for curative determination, monitoring and prognosis of cancer tumor [24]. Herein, we fabricated a new electrochemical immunosensor for determination of CEA, as a model analyte, based on organic–inorganic hybrid magnetic nanocomposites as matrices and nanogold-decorated graphene nanosheets as the label of secondary antibody. The immunosensor was prepared by immobilizing anti-CEA antibody on nanosilver-patterned PPD-functionalized magnetic beads. The doped PPD acted as not only a cross-linkage but also a mediator for the electron transfer. With the sandwich-type immunoassay mode, the assay was performed by using the labeled horseradish peroxide on the secondary antibody as trace tags. Related experiment details were described as follows.

2. Experimental

2.1. Materials and reagent

Mouse monoclonal anti-CEA (clone C6G9), horseradish peroxidase-anti-CEA conjugates (HRP-anti-CEA), and CEA standards (0, 5, 10, 20, 40 and 80 ng mL^{-1}) were purchased from Biocell Biotechnol. Co. Ltd. (Zhengzhou, China). *o*-Phenylenediamine (98%, w/w), $HAuCl_4{\cdot}4H_2O$ and bovine serum albumin (BSA) (96–99%) were obtained from Sigma–Aldrich (USA). Graphene oxide nanosheets were prepared and characterized as described in the previous published paper [25]. Magnetic Fe_3O_4 nanoparticles (MB, particle size: 100 nm) in an aqueous suspension with a concentration of 25 mg mL^{-1} were obtained from Chemicell GmbH (Berlin, Germany). Carbon graphite powder (<325 mesh, Johnson Matthey) and paraffin oil (Fluka) were used for the preparation of carbon paste electrode. Prior to the preparation, the graphite powder was treated at 700 °C for 30 s in a muffle furnace. All other reagents were of analytical grade and were used without further purification. Ultrapure water obtained from a Millipore water purification system (≥18 MΩ, Milli-Q, Millipore) was used in all runs. Acetic acid salt-buffered saline (ABS, 0.1 M) solution of various pH-values was prepared and 0.1 M KCl was used as the supporting electrolyte.

2.2. Patterning nanosilver particle assembly on poly(o-phenylenediamine)-functionalized magnetic beads (AgNP–PPD–MB)

Prior to experiment, a magnetic carbon paste electrode (MCPE) was prepared. Initially, 1.0 mL of paraffin oil was added into 3 g of graphite powder, and the resulting mixture was then stirred thoroughly. Following that, a glass tube (5 mm in diameter and 20 mm in depth) was initially filled with a magnet (5 mm in diameter and 2 mm in depth, to produce an inhomogeneous magnetic density, 0.2 T at the surface), then a portion of resulting paste was put into the glass tube with electrical contact, in the meantime, a copper wire was inserted into the back of mixture. The obtained MCPE was dried and stored for one day at 4 °C. After the electrode tip was gently rubbed on a fine paper to produce a flat surface and cleaned with doubly distilled water, 5 μL of magnetic Fe_3O_4 suspension (25 mg mL^{-1}) were dropped on the surface of MCPE. With the aid of the external magnet, magnetic beads (MBs) were immobilized on the MCPE.

Next, the MB-functionalized MCPE was immersed into 1.0 M H_2SO_4 solution containing 0.1 M *o*-phenylenediamine monomer, and the voltammetric scanning was carried out from −0.6 V to 1.3 V (*vs.* SCE) at 100 mV s^{-1} for 25 cycles. During this process, the *o*-phenylenediamine was electrochemically polymerized onto the MB/MCPE. Consequently, silver nanoparticles were also electrochemically deposited on the PPD/MB/MCPE by a potential scan from −1.5 to 0 V for 10 cycles at 100 mV s^{-1} into another mixture containing 5.0 mM $AgNO_3$ containing 0.1 M KNO_3. The silver-deposited PPD/MB/MCPE (designated as AgNP/PPD/MB/MCPE) was taken out from the solution and thoroughly rinsed with water. Then, modification by anti-CEA antibody was performed by soaking the AgNP/PPD/MB/MCPE into 500 μL of 1 mg mL^{-1} anti-CEA solution for 4 h. The obtained immunosensor (designated as anti-CEA/AgNP/PPD/MB/MCPE) was immersed into 2.5 wt% BSA solution, and incubated for 1 h at room temperature (RT) to block possible remaining active sites of nanomaterials and avoid the non-specific adsorption. The resulting immunosensor was stored at 4 °C when not in use. The fabricated procedure is shown in Scheme 1a.

2.3. Synthesis and bioconjugation of nanogold-coated graphene oxide nanosheets (AuNP-GO)

Graphene coated with gold nanoparticles (AuNP-GO) were synthesized according to the literature with a little modification [26], as schematically illustrated in Scheme 1b. 10 mg of graphene oxide nanosheets was initially dispersed into 25 mL of distilled water, and then the mixture was sonicated at RT until a homogeneous solution was obtained. Following that, 1.0 mL of 1.0 wt% chloroauric acid and 1.0 g of NaOH solid powder were quickly added into the mixture in turn. And then the obtained mixture was sonicated for another 2 h at RT to make the $[AuCl_4]^-$ ions attach onto the graphene nanosheets. With the aid of graphene oxide nanosheets, the Au(III) was *in situ* reduced to the zero-valent gold nanoparticles. Free gold nanoparticles were removed by centrifugation at 6000 × *g* for 10 min, and the obtained precipitate (designated as AuNP-GO) was dissolved into 3 mL distilled water for further use.

Prior to experiment, 300 μL of HRP-anti-CEA (0.1 mg mL^{-1}) was added into the above solution. The mixture was slightly shaken for 5 min, and transferred to the refrigerator for further reaction for 6 h. Following that, the suspension was centrifuged at 4 °C for 20 min at 10,000 rpm. The obtained AuNP-GO nanosheets labeled with HRP-anti-CEA (designated as HRP-anti-CEA/AuNP-GO) were dispersed in 3 mL of distilled water containing 1.0 wt% BSA and stored at 4 °C until use. For comparison, HRP-anti-CEA-conjugated AuNPs (HRP-anti-CEA/AuNP) and HRP-anti-CEA-conjugated GO

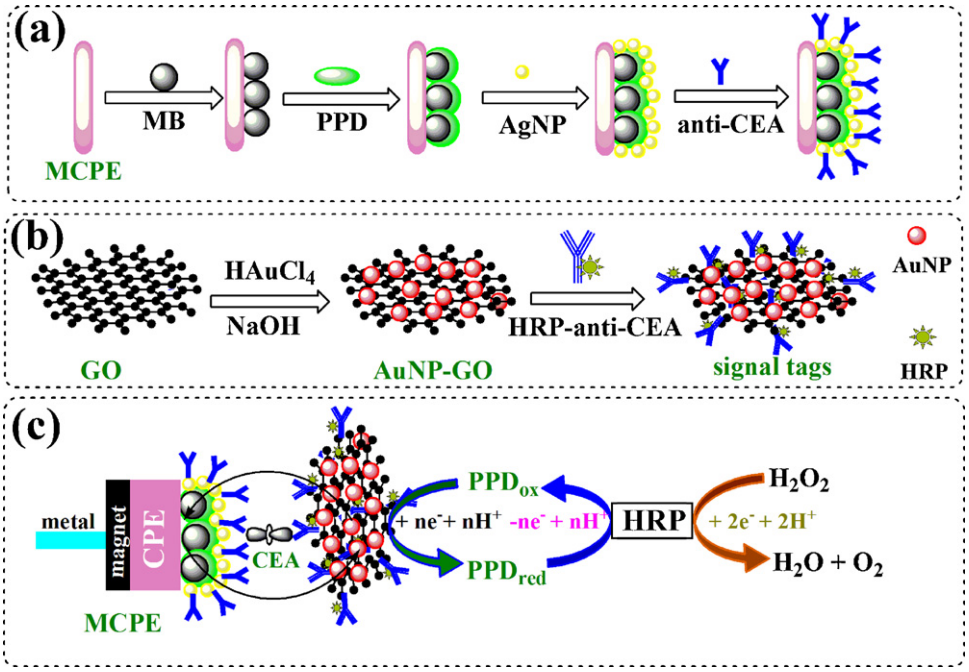

Scheme 1. Schematic illustration of (a) HRP-anti-CEA/AuNP-GO signal tags, (b) the magnetic immunosensor, and (c) measurement principle of the electrochemical immunoassay.

(HRP-anti-CEA/GO) were prepared based on direct absorption and glutaraldehyde linkage.

2.4. Electrochemical immunoassay procedure

The analytical procedure for electrochemical immunoassay of CEA is schematically depicted in Scheme 1c. All electrochemical measurements were carried out on a CHI 630D Electrochemical Analyzer (CH Instruments Inc., Shanghai, China) using a modified MCPE working electrode, a platinum wire auxiliary electrode and a SCE reference electrode. The assay procedure was depicted as follows. After incubating the immunosensor into incubation solution containing various concentrations of CEA (*Note*: Sample matrix component was blank human serum) for 17 min at RT and washing with distilled water, the resulting substrates were submerged in another incubation solution containing HRP-anti-CEA/AuNP-GO for another 17 min at RT. After rinsing thoroughly with distilled water to remove the unbound biomolecules, a differential pulse voltammetric (DPV) measurement from −200 to −850 mV (*vs.* SCE) with a pulse amplitude of 50 mV and a pulse width of 50 ms was registered as the sensor signals in pH 5.3 acetic acid buffer containing 3 mM H_2O_2 due to the catalytic reduction of the bound HRP toward H_2O_2 in the presence of PPD.

After each immunoassay run, the immunosensors were regenerated by immersing into 0.1 M glycine–HCl (pH 2.0) for 5 min to break the antigen–antibody linkage while the regeneration of the electrode was carried out by turning the nut to extrude the paste layer and then polishing with a fine paper to produce a smooth shiny surface. All incubations and measurements were performed at RT. Analyses were always made in triplicate.

3. Results and discussion

3.1. Characteristics of AgNP–PPD–MB and AuNP-GO nanocomposites

Fig. 1a shows the transmission electron microscope (TEM, H600, Hitachi Instrument, Japan) of AgNP–PPD–MB, and the mean size was 130 nm, which was obviously larger than 100 nm. The increase in size was mainly attributed to the assembly of silver nanoparticles on the surface of magnetic beads. Meanwhile, we could also clearly observe many small-sized nanoparticles coated on the surface of nanocomposites. The result revealed that silver nanoparticles could be formed on the MBs by using PPD as bridges. The reason might be the fact that Ag(I) can be jointed by amino-groups. The amino and the adjacent imino easily formed a stable network complex structure with the Ag(I) while making the reduction of the oxidative ions through complexation [27]. The redox aromatic diamine polymers successfully achieved the aim of adsorbing a mass of silver metal ions and formed sliver nanoparticles on the PPD. In addition, the unique trapezoidal, semi-ladder structure of the PPD could make them better load and avoid migration or reunion of the nanoparticles effectively. Fig. 1b displays the typical TEM image of the synthesized AuNP-GO. Comparing to pure graphene oxide reported previously [28], many gold nanoparticles were homogeneously dispersed on the graphene nanosheets. The presence of nanogold and nanosilver particles provided a large surface area for the conjugation of the biomolecules.

To further monitor the formation of AgNP–PPD–MB and AuNP-GO, UV–vis absorption spectrometry (UV 1102, Tianmei, China) was used to characterize the synthesized nanostructures (Fig. 2). The UV–vis absorption spectra of magnetic Fe_3O_4 nanoparticles were complicated, and the absorbance increased with the wavelength decreased in the range of 800–200 nm [29]. When a layer of *o*-phenylenediamine was electrochemically polymerized on the magnetic beads, an obvious absorption peak at 475 nm was observed (Fig. 2a), which was in accordance with the reported result [30]. The presence of poly(*o*-phenylenediamine) could provide a biocompatible microenvironment for the immobilization of silver nanoparticles since the poly(*o*-phenylenediamine) has strong affinity capacity for heavy metals, such as Ag(I) [27]. During the polymerization process, although many *o*-phenylenediamine molecules were electropolymerized together, some uncombined amidogens could be exposed outside of the polymer. Significantly, another absorption peak at 398 nm was appeared after the formation of AgNP–PPD–MB (Fig. 2b), indicating the successful synthesis

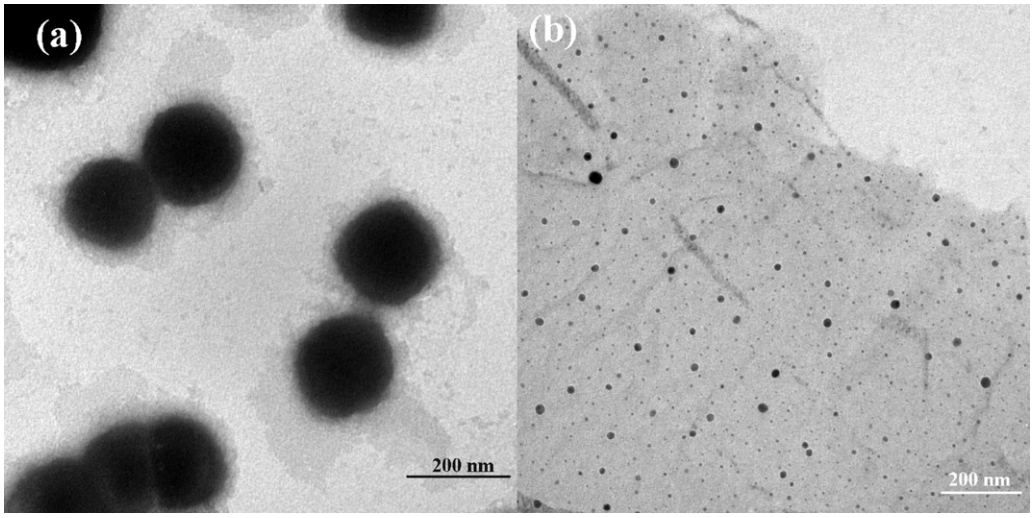

Fig. 1. TEM images of: (a) Ag–PPD–MB and (b) AuNP-GO.

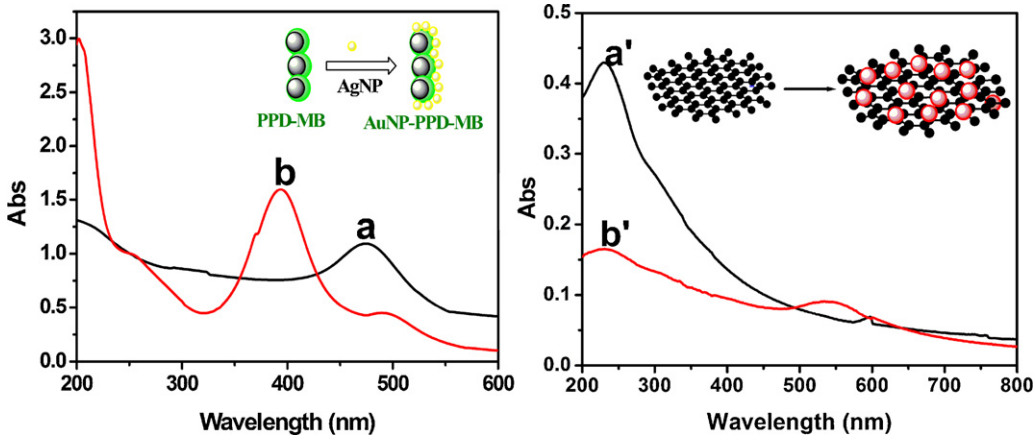

Fig. 2. UV–vis absorption spectra of: (a) PPD–MB, (b) AgNP–PPD–MB, (a′) graphene oxide, and (b′) AuNP-GO.

of silver nanoparticles [31]. Following that, anti-CEA antibodies could be conjugated onto the surface of AgNP–PPD–MBs through the interaction between AgNPs and the —SH/or —NH_2 groups of anti-CEA. In addition, we also utilized UV–vis absorption spectrometry to investigate the as-prepared AuNP-GO nanocomposites. As seen from Fig. 2a′, there was an absorption peak at 227 nm for the graphene oxide nanosheets. However, when gold nanoparticles were *in situ* synthesized on the graphene oxide nanosheets, two absorption peaks at 534 nm and 238 nm were simultaneously acquired (Fig. 2b′). The existence of the new peak at 534 nm revealed the presence of gold nanoparticles [32]. The absorption peak at 238 nm was ascribed to the typical carbonyl groups on the GO. However, the absorption wavelength was obviously red shift in contrast with that of pure graphene oxide at 227 nm. The reason might be the fact that the formation of AuNP-GO decreased the excited energy of carbonyl groups from n orbital to π^* orbital [33]. The results indicated that the Au(III) could be reduced to Au^0 under the wild conditions.

3.2. Electrochemical characteristics of the magnetic immunoassays

Fig. 3 displays the cyclic voltammograms of the magnetic immunoassay after each step in ABS, pH 5.3 at 50 mV s^{-1}. No peak was observed at MB-modified MCPE in the applied potential (Fig. 3a). When *o*-phenylenediamine monomers were electropolymerized on the MB/MCPE, a couple of redox peak at −600 and −480 mV was achieved (Fig. 3b). The result indicated that the formation of poly(*o*-phenylenediamine) did not change its redox properties, which could act as a mediator for electron transfer

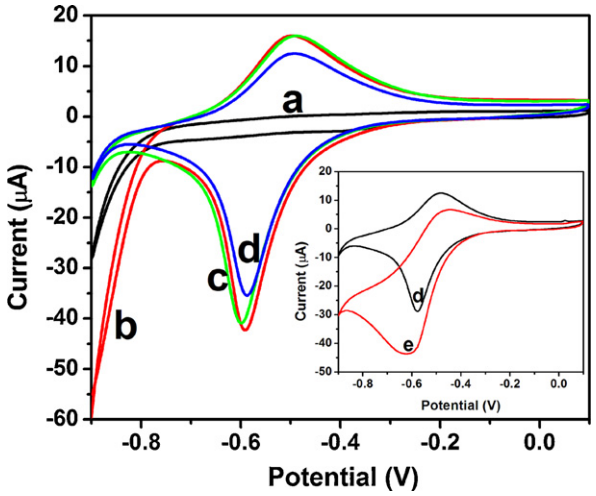

Fig. 3. Cyclic voltammograms of (a) MB/MCPE, (b) PPD/MB/MCPE, (c) AgNP/PPD/MB/MCPE, (d) anti-CEA/AgNP/PPD/MB/MCPE in pH 5.3 ABS, and (e) cyclic voltammograms of the electrode '*d*' after incubation with 10 ng mL^{-1} CEA and excess HRP-anti-CEA/AuNP-GO in pH 5.3 ABS containing 3 mM H_2O_2.

between the solution and the base electrode. The processes of reduction reactions for the PPD could be illustrated as follows:

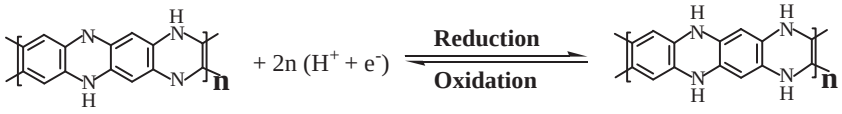

(1)

Although the residual amino groups on the poly(*o*-phenylenediamine) could be used for the conjugation of biomolecules by using the cross-linking reaction, the immobilized amount was limited. The assembly of silver nanoparticles on the PPD/MB/MCPE could provide a large surface coverage for the immobilization of biomolecules. Significantly, the redox peak current did not decrease in comparison with those of the PPD/MB/MCPE after the formation of AgNP/PD/MB/MCPE (Fig. 3c). As shown in Fig. 3d, after immobilization of anti-CEA antibody, the peak current was decreased. This phenomenon might be attributed to introduction of anti-CEA biomacromolecules in the complex membrane.

To investigate the bioactivity of the immobilized anti-CEA on the magnetic beads, the as-prepared immunosensor was used for detection of 10 ng mL^{-1} CEA (as an example) by using HRP-anti-CEA/AuNP-GO as secondary antibodies. As shown in Fig. 3e, the peak currents were decreased obviously in comparison with anti-CEA/AgNP/PPD/MB/MCPE (Fig. 3d), suggesting that the formed immunocomplex on the MCPE hindered the electron transfer. After H_2O_2 was added into the pH 5.3 ABS, an obvious catalytic characteristic with a distinct increase of the reduction current and a decrease of the oxidation current was observed (Fig. 3e). The result indicated that the immobilized HRP molecules on the HRP-anti-CEA/AuNP-GO still retained high enzymatic activity. Therefore, the as-prepared magnetic immunosensor could be applied for determination of CEA.

The proposed reaction scheme for HRP-PPD is depicted in Scheme 1c. HRP converts molecular hydrogen peroxide to water and oxygen oxidizing the PPD matrix simultaneously. The reduced state of the polymer is recovered by the Nernstian equilibrium. The polymer reduction step causes current flow through the electrode. The catalytic cycle closes by the reoxidation of the polymer by HRP [34].

3.3. Comparison of various immunosensing interfaces

To investigate the effect of various immunosensing interfaces on the electrochemical properties of the magnetic immunoassays, we prepared four types of immunosensors, such as anti-CEA/MB/MCPE (Preparation method was described in our previous report [29]), anti-CEA/PPD/MB/MCPE (using glutaraldehyde as cross-linkage reagent), anti-CEA/AgNP/MB/MCPE (using the opposite-charged adsorption technique between AuNPs and MBs), and anti-CEA/AgNP/PPD/MB/MCPE for detection of various CEA concentrations with the same assay mode using HRP-anti-CEA/AuNP-GO as secondary antibodies. *o*-Phenylenediamine was added into the detection solution when using anti-CEA/MB/MCPE and anti-CEA/AgNP/MB/MCPE as sensing interface. The optimal principle for various immunosensing interfaces was based on the shift in the cathodic current relative to zero analyte. As shown in Fig. 4A, an optimal current response was found at the anti-CEA/AgNP/PPD/MB/MCPE. Several possible explanations might be attributed to the observation: (i) PPD with high conductivity and good redox properties could provide a convenience for electrochemical measurement; (ii) PPD complex membrane had a mesoporous and branched structure with many residual amino groups, which could increase the surface area of the modified electrode and enhance the immobilized amount of biomolecules; (iii) Silver nanoparticles with good biocompatibility and excellent conductivity favored for the biomolecular conjugation, and facilitated the electron communication with the base electrode. Therefore, nanosilver and PPD were used for the fabrication of the magnetic immunosensors.

3.4. Comparison of various secondary antibodies

In the sandwich-type immunoassays, the detectable signal mainly derives from the labeled signal tags on the secondary antibodies. In this study, the signal tags, *i.e.* HRP molecules, were initially labeled to anti-CEA antibody, and then the HRP-anti-CEA conjugates were relabeled to the AuNP-GO. Could AuNP-GO enhance the signal of the electrochemical immunosensor? We also prepared three types of signal tags, *i.e.* HRP-anti-CEA/AuNP-GO, HRP-anti-CEA-labeled AuNPs, and HRP-anti-CEA-conjugated GO, which were employed for determination of CEA on the anti-CEA/AgNP/PD/MB/MCPE. The assay was based on the aforementioned principle. As seen from Fig. 4B, the simultaneous existence of AuNPs and GO could obviously improve the electrochemical response of the immunosensor. The reason might be attributed to the following issues: (i) The absence of gold nanoparticles, *i.e.* direct conjugation of HRP-anti-CEA on the graphene, might decrease the immobilized amount of biomolecules compared with the presence of nanogold particles; (ii) graphene oxide with three-dimensional nanosheets could immobilize much more gold nanoparticles than signal gold nanoparticle, thus indirectly increasing the conjugation of HRP-anti-CEA on the graphene.

3.5. Optimization of assay conditions

To achieve an optimal analytical property of the as-prepared immunosensor, some conditions including incubation temperature, incubation time (*i.e.* response time) and pH of assay solution should be investigated. Considering the convenient operation and practical application of the immunosensor, all experiments were carried out at room temperature (25 ± 1.0 °C). At this condition, we investigated the effect of various incubation times on the current of the immunoassay using 5 ng mL^{-1} CEA as an example. As shown in Fig. 5a, the reduction currents increased with the increment of incubation time, finally, trended to level off after 17 min. Longer incubation time did not improve the signal. Therefore, 17 min was used for the antigen–antibody reaction.

Fig. 5b shows the effect of pH of ABS on the current responses of the immunosensor. The optimal current response was obtained at pH 5.3 ABS. Actually, the reaction of the PPD in the electrochemical process involved additional protonation/deprotonation transition and exhibited better electrochemical performance in acidic electrolyte than in alkaline one [35]. In addition, considering the bimolecular activity, pH of the ABS could not be too low. So, pH 5.3 ABS was used as supporting electrolyte for detection of CEA.

3.6. Analytical performance of the magnetic immunoassay

Under optimal conditions, the sensitivity and dynamic range of the magnetic immunoassay was evaluated toward CEA standards. As shown in Fig. 6, the peak current of the magnetic immunosensor increased with the increscent of CEA concentration and exhibited a wide linear dynamic range of 0.01–40 ng mL^{-1} with a low detection

Table 1
Comparison of analytical properties of variously electrochemical immunosensors toward CEA.

Electrochemical immunosensor[a]	Dynamic range (ng mL^{-1})	LOD (ng mL^{-1})	Ref.
Anti-CEA/CS-CNTs-AuNP/GCE	0.1–2.0, 2.0–200	0.04	[36]
HRP-anti-CEA-NGGNs	0.05–350	0.01	[37]
Anti-CEA/AuNP/CNTs/(PSS/PDDA/CNTs)$_2$/GCE	0.1–2, 2–160	0.06	[38]
Anti-CEA/(AuNP)$_n$Au/Fe_3O_4 nanoparticle/SPCE	0.005–50	0.001	[39]
Core-Shell Fe_3O_4@silver	1.5–200	0.5	[29]
Anti-CEA/AuNP/TH/NF	0.01–12	0.005	[40]
HRP-anti-CEA/AuNP/Fe_3O_4-CS/PB/GCE	0.1–220	0.01	[41]
CEA/AgNP/DNA/TH/NF/SCPE	0.03–32	0.01	[42]
Anti-CEA/AgNP/PPD/MB/MCPE	0.01–40	0.001	This work

[a] CS, chitosan; CNT, carbon nanotube; GCE, glassy carbon electrode; NGGN, nanogold-enwrapped graphene nanosheets; PSS, poly(sodium-*p*-styrene-sulfonate); PDDA, poly(diallyldimethylammonium chloride); SPCE, screen-printed carbon electrode; TH, thionine; NF, Nafion; PB, prussian blue.

limit of 0.001 ng mL^{-1} CEA at a signal-to-noise ratio of 3. The linear regression equation is i_{pc} (μA) = −28.32 to −1.332 × Ln $C_{[CEA]}$ (ng mL^{-1}, R^2 = 0.991). The dynamic range of the electrochemical immunoassay was acceptable and could be further used for practical application. In addition, the analytical properties of the electrochemical immunosensor were compared with other CEA immunosensors or immunoassays (Table 1). The results indicated that the electrochemical immunoassay enabled available linear ranges and low LOD.

3.7. Precision, reproducibility, selectivity and stability of the magnetic immunoassay

The precision and reproducibility of the magnetic immunoassay were evaluated by using the variation coefficient (CV) of the intra- and inter-assay (CV, n = 3). The experimental results indicated that the CVs of the assays using the immunosensors with the same batch were 9.2%, 8.5% and 9.6% at the 0.01 ng mL^{-1}, 5 ng mL^{-1}, and 40 ng mL^{-1} CEA levels, respectively. And the sensor-to-sensor reproducibility with various batches was monitored, and the CVs were 7.7%, 9.3% and 8.4% at the above mentioned levels, respectively. Hence, the precision and reproducibility of the magnetic immunoassay was acceptable.

To investigate the interfering effects of sample matrix components on the electrochemical responses of the developed immunoassays, we challenged the system with several possible components in human serum, such as K^+, Ca^{2+}, Cl^-, HCO_3^-, glucose (Glu), uric acid (UA), dopamine (DA), and cancer antigen 125 (CA125). These samples were assayed by spiking them into blank human serum. The comparative study was carried out by measuring the low concentration of CEA analyte and high concentration of interfering components. As indicated from Fig. 7, higher current

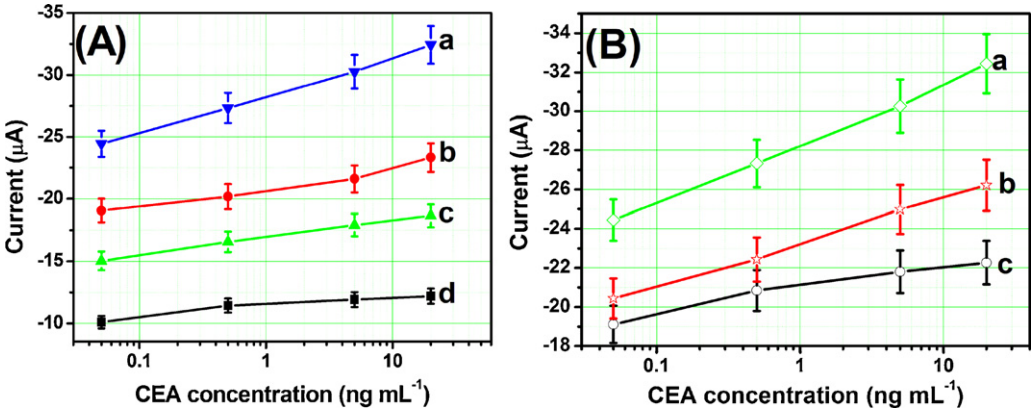

Fig. 4. Effect of: (A) various immunosensing interfaces: (a) anti-CEA/AgNP/PPD/MB/MCPE, (b) anti-CEA/PPD/MB/MCPE, (c) anti-CEA/AuNP/MB/MCPE and (d) anti-CEA/MB/MCPE on the electrochemical signal of the magnetic immunoassay using HRP-anti-CEA/AuNP-GO as trace tags, and (B) various signal tags: (a) HRP-anti-CEA/AuNP-GO, (b) HRP-anti-CEA/AuNP, and (c) HRP-anti-CEA/GO on the electrochemical signal of the magnetic immunoassay using anti-CEA/AgNP/PD/MB/MCPE as immunosensing probe toward various concentrations of CEA standards.

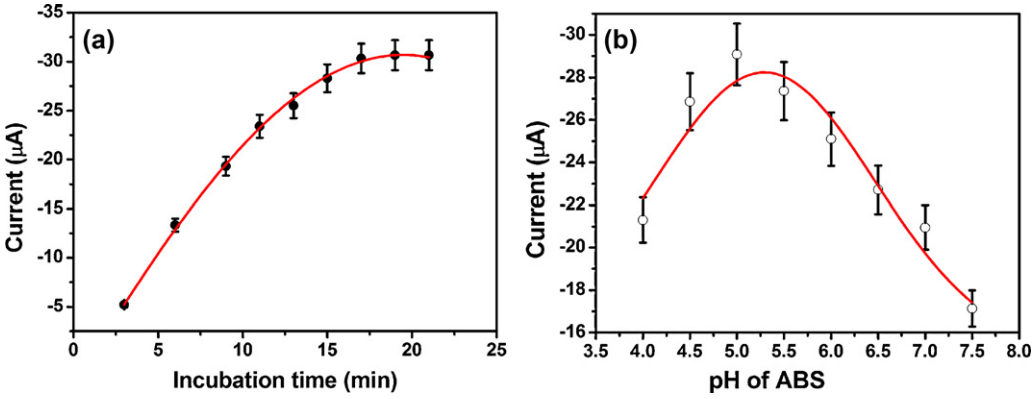

Fig. 5. Effects of: (a) incubation time and (b) pH of ABS on the electrochemical responses of the magnetic immunoassay.

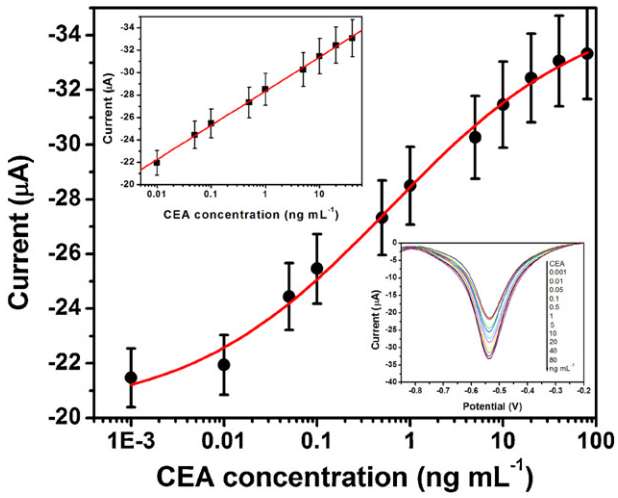

Fig. 6. Calibration plots of the magnetic immunoassay toward CEA standards in pH 5.3 ABS containing 3.0 mM H_2O_2. *Inset:* linear and DPV curves.

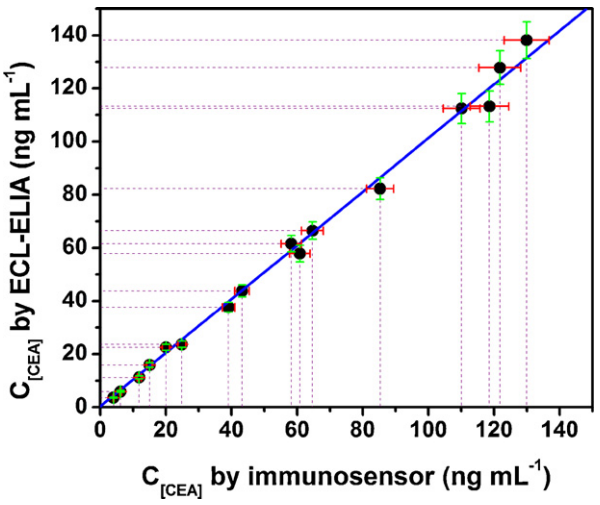

Fig. 8. Comparison of assay results for 16 human serum specimens by using the electrochemical immunoassay and commercially available ECL-ELIA.

was observed with the target CEA than those of other components. These results clearly demonstrated the high specificity of the electrochemical immunosensors. In addition, the stability of the immunosensor was satisfactory, and as much as 88.7% of the initial peak current was preserved after storage of the immunosensor and signal tags at 4 °C for 30 days.

3.8. Evaluation of real samples and method comparison

To further investigate the analytical reliability of the magnetic immunoassay, the immunosensor was applied for determination of 16 real serum specimens, and the assayed results were compared with those obtained by a commercially available Electrochemiluminescent enzyme-linked immunoassay (ECL-ELIA) (*Note*: an appreciate dilution by using distilled water was preferable when the concentration of CEA was too high). Comparison of the experimental results obtained by the proposed immunosensor with those of ECL-ELIA was performed *via* a regression method (Fig. 8). The regression line was fitted to $y = (1.025 \pm 0.15)x - (0.765 \pm 3.2)$ ($R^2 = 0.995$), where x stands for the CEA concentrations estimated with the electrochemical immunosensor and y stands for those of the reference procedure. No significant differences were encountered between the optimum values of intercept and slope, thereby revealing a good agreement between both analytical methods. Thus, we might utilize the magnetic immunoassay for detection of CEA in clinical diagnostics.

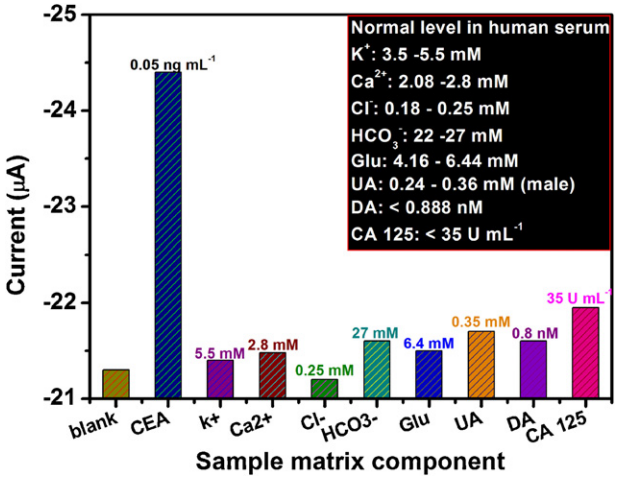

Fig. 7. The interfering effects of sample matrix components on the currents of the immunosensors.

4. Conclusions

In summary, this work reports a simple and facile route for the synthesis of a new magnetic nanocomposite with redox activity and good biocompatibility, and its possible application in the electrochemical immunoassays. Experimental results indicated that the magnetic immunosensors could exhibit high sensitivity, good reproducibility, and acceptable selectivity. Compared with our previously reported magnetic immunoassays [43,41,44], the developed magnetic immunoassays have several merits as follows: (i) The redox electroactive species can be efficiently encapsulated into the magnetic nanocomposites, facilitate the electrochemical measurement, and avoid the contamination of the electron mediators in the detection solution; (ii) The synthesized poly(*o*-phenylenediamine) polymers with the trapezoidal and semi-ladder structures can provide a large surface coverage for the patterning of silver nanoparticles; (iii) Graphene nanosheets with two-dimensional nanostructures are used for the immobilization of gold nanoparticles and multiple biomolecules, which enhances the possibility of antigen–antibody interaction. Importantly, the methodology can be readily extended for use with other cancer markers by controlling the target antibody, and thus represents a universal and versatile detection method.

Acknowledgements

Support by the National Natural Science Foundation of China (nos. 21075019, and 41176079), the Research Fund for the Doctoral Program of Higher Education of China (no. 20103514120003), the National Science Foundation of Fujian Province (no. 2011J06003), and the "973" National Basic Research Program of China (no. 2010CB732403) is gratefully acknowledged.

References

[1] B. Li, W. Zhong, J. Mater. Sci. 46 (2011) 5595.
[2] Y. Zhang, L. Wang, J. Tian, H. Li, Y. Luo, Y. Sun, Langmuir 27 (2011) 2170.
[3] A. Sionkowaska, Prog. Polym. Sci. 36 (2011) 1254.
[4] P. Dallas, V. Sharma, R. Zboril, Adv. Colloid Interface Sci. 166 (2011) 119.
[5] M. Zhu, G. Diao, Nanoscale 3 (2011) 2748.
[6] G. Wang, X. Su, Analyst 136 (2011) 1783.

[7] P. Howes, M. Green, A. Bowers, D. Parker, G. Varma, M. Kallumadil, M. Hughes, A. Warley, A. Brain, R. Botnar, J. Am. Chem. Soc. 132 (2010) 9833.
[8] S. Behrens, Nanoscale 3 (2011) 877.
[9] J. Liu, S. Qiao, Q. Hu, G. Lu, Small 7 (2011) 425.
[10] A. Gijs, F. Lacharme, U. Lehmann, Chem. Rev. 110 (2010) 1518.
[11] S. Shylesh, V. Schunemann, W. Thiel, Angew. Chem. Int. Ed. 49 (2010) 3428.
[12] T. Prasad, V. Kambala, R. Naidu, Curr. Nanosci. 7 (2011) 531.
[13] M. Rycenga, C. Cobley, J. Zeng, W. Li, C. Moran, Q. Zhang, D. Qin, Y. Xia, Chem. Rev. 111 (2011) 3669.
[14] P. Rijiravanich, M. Somasundrum, W. Surareungchai, Anal. Chem. 80 (2008) 3904.
[15] D. Chirizzi, C. Malitesta, Sens. Actuators B 157 (2011) 211.
[16] C. Wu, H. Chang, Anal. Chim. Acta 505 (2004) 239.
[17] J. Kan, Y. Jiang, Y. Zhang, Mater. Chem. Phys. 102 (2007) 260.
[18] N. Blinova, P. Bober, J. Hrom, M. Trchov, J. Stejskal, J. Prokes, Polym. Int. 58 (2010) 437.
[19] R. Garjonyte, A. Malinauskas, Sens. Actuators B 56 (1999) 85.
[20] M. Shi, Y. Peng, J. Zhou, Biosens. Bioelectron. 22 (2007) 2841.
[21] M. Huang, Q. Peng, X. Li, Chem. Eur. J. 12 (2006) 4341.
[22] X. Li, X. Ma, J. Sun, M. Huang, Langmuir 25 (2009) 1675.
[23] J. Ho, Y. Lin, L. Wang, K.U. Hwang, P. Chou, Anal. Chem. 81 (2009) 1340.
[24] N. Berois, M. Varangot, B. Aizen, R. Estrugo, L. Zarantonelli, P. Fernandez, G. Krygier, F. Simonet, E. Barrios, I. Muse, E. Osinaga, Eur. J. Cancer 36 (2000) 717.
[25] C. Lu, H. Yang, C. Zhu, X. Chen, G. Chen, Angew. Chem. Int. Ed. 28 (2009) 4785.
[26] X. Chen, G. Wu, J. Chen, X. Chen, Z. Xie, X. Wang, J. Am. Chem. Soc. 133 (2011) 3693.
[27] X. Li, M. Huang, S. Li, Acta Mater. 52 (2004) 5363.
[28] Q. Li, D. Tang, J. Tang, B. Su, G. Chen, M. Wei, Biosens. Bioelectron. 27 (2011) 153.
[29] D. Tang, R. Yuan, Y. Chai, J. Phys. Chem. B 110 (2006) 11640.
[30] P. Gajendran, R. Saraswathi, J. Phys. Chem. C 111 (2007) 11320.
[31] A. Sachdeva, S. Sodaye, A. Pandey, A. Goswami, Anal. Chem. 78 (2006) 7169.
[32] D. Tang, R. Yuan, Y. Chai, Anal. Chem. 80 (2008) 1582.
[33] K. Putz, O. Compton, C. Segar, Z. An, S. Nguyen, L. Brinson, ACS Nano 5 (2011) 6601.
[34] B. Palys, A. Bokun, J. Rogalski, Electrochim. Acta 52 (2007) 7075.
[35] W. Long, P. Rhodes, L. Young, R. Rolison, Nano Lett. 3 (2003) 1155.
[36] X. Gao, Y. Zhang, Q. Wu, H. Chen, Z. Chen, X. Lin, Talanta 85 (2011) 1980.
[37] Z. Zhong, W. Wu, D. Wang, J. Shan, Y. Qing, Z. Zhang, Biosens. Bioelectron. 25 (2010) 2379.
[38] X. Gao, Y. Zhang, H. Chen, Z. Chen, X. Lin, Anal. Biochem. 414 (2011) 70.
[39] J. Li, H. Gao, Z. Chen, X. Wei, C. Yang, Anal. Chim. Acta 665 (2010) 98.
[40] Q. Li, D. Tang, J. Tang, B. Su, J. Huang, G. Chen, Talanta 84 (2011) 538.
[41] H. Chen, J. Tang, B. Su, G. Chen, J. Huang, D. Tang, Anal. Chim. Acta 678 (2010) 169.
[42] W. Wu, P. Yi, P. He, T. Jing, K. Liao, K. Yang, H. Wang, Anal. Chim. Acta 673 (2010) 126.
[43] J. Tang, D. Tang, R. Niessner, G. Chen, D. Knopp, Anal. Chem. 83 (2011) 5407.
[44] B. Zhang, D. Tang, B. Liu, H. Chen, Y. Cui, G. Chen, Biosens. Bioelectron. 28 (2011) 174.